Applied Catalysis B: Environmental 96 (2010) 421–433

Contents lists available at ScienceDirect

Applied Catalysis B: Environmental

journal homepage: www.elsevier.com/locate/apcatb

Effect of water vapor on the activity and stability of Pd/SZ and Co/ZrO_2 in dual-catalyst treatment of simulated exhaust from lean-burn natural gas engines

Burcu Mirkelamoglu, Umit S. Ozkan*

140 W. 19th Avenue, Department of Chemical and Biomolecular Engineering, The Ohio State University, Columbus, OH 43210, USA

ARTICLE INFO

Article history:
Received 16 December 2009
Received in revised form 19 February 2010
Accepted 25 February 2010
Available online 6 March 2010

Keywords:
Lean NOx reduction
NO oxidation
Sulfated zirconia
Palladium
Cobalt

ABSTRACT

A dual-catalyst system, consisting of an NO oxidation catalyst component (Co/ZrO_2) and a NOx reduction catalyst component (Pd/SZ) was investigated for selective catalytic reduction of NOx under lean conditions. The integrated catalyst system is capable of performing three-distinct catalytic functions, namely, NOx reduction, combustion of unburned hydrocarbons and oxidation of carbon monoxide. The hydrothermal stability of the dual-catalyst system was investigated through steady-state and time-on-stream measurements. Water vapor was found to inhibit the NOx reduction activity of Pd/SZ, whereas it had no effect on NO oxidation over Co/ZrO_2. The dual-catalyst system was capable of retaining stable catalytic activity during simulated lean exhaust treatment in the presence of 7% H_2O.

1. Introduction

Lean-burn natural gas reciprocating engines constitute a well-understood, simple and inexpensive technology that reaches higher efficiencies and produces significantly cleaner exhaust emissions than the rich-burn alternatives [1]. These engines are increasingly popular for distributed power generation. Lean-burn operation results in cleaner engine-out exhaust, but the exhaust stream still contain significant levels of carbon monoxide, unburned hydrocarbons and nitrogen oxides (NOx). The current aftertreatment technologies for emissions abatement from stationary sources utilize NH_3 as the reducing agent, but these technologies have several drawbacks concentrated around ammonia slip and direct oxidation, corrosion of the downstream equipment due to ammonium salts, and infrastructure requirements [2]. The three-way catalyst technology used in mobile applications is unsuitable for lean-burn natural gas engines since it is ineffective under lean-burn conditions [3]. Significant research efforts have been devoted to the development of aftertreatment technologies that would utilize unburned hydrocarbons that are available in the exhaust stream as the reducing agents for NOx reduction. Methane has attracted particular attention as the reducing agent since it is readily available as the major component of natural gas and it is the least expensive lower hydrocarbon. Although methane is readily available, effective utilization of methane as the reducing agent in a hydrocarbon–SCR system is a significant challenge due to the difficulty of activating methane and the competition from combustion of the hydrocarbon in the presence of excess oxygen [4,5].

Palladium-based catalysts supported on zeolites and other acidic supports are among the most widely studied catalysts for selective catalytic reduction of NOx with CH_4 under lean conditions [6]. Nishizaka and Misono [7,8] were the first to report a link between the acidity of the support and activity in NOx reduction. Later it was established by a number of studies that Pd^{2+} ions were the active sites for the NOx reduction reaction [9] whereas, PdO aggregates showed activity for CH_4 combustion [10,11]. The role of acidic supports in stabilizing palladium in the form of Pd^{2+} ions was shown by Resasco and coworkers [9]. Further work by Resasco and coworkers [12] showed that protons associated with surface sulfate groups served as anchoring sites for Pd^{2+} ions over Pd/SZ. Although zeolite-supported Pd catalysts showed high CH_4–SCR activity, the major drawback of these catalysts was their poor stability under reaction conditions. Studies on the deactivation of zeolite-supported Pd catalysts showed agglomeration of bulky PdO particles outside the zeolite pores by hydrothermal treatment [13,14] and by extended time-on-stream [11,15,16]. On most of the zeolite systems, leaching of aluminum under hydrothermal conditions from tetrahedral sites within the zeolite framework to locations in zeolite pores was reported to result in the formation of PdO aggregates and loss of metal dispersion [17]. Sulfated zirconia (SZ) supported palladium catalysts showed better hydrothermal

* Corresponding author. Tel.: +1 614 292 6623; fax: +1 614 292 3769.
E-mail address: ozkan.1@osu.edu (U.S. Ozkan).

0926-3373/$ – see front matter © 2010 Elsevier B.V. All rights reserved.
doi:10.1016/j.apcatb.2010.02.040

stability than their zeolite-based counterparts [18]. Quincoces et al. [19] reported a reversible decrease in both NO reduction and CH_4 combustion activity of Pd–Co/SZ in the presence of water vapor accompanied with a shift in the optimum operating temperature to higher temperatures. Figueras et al. [20] showed that water resulted in a reversible decrease in the NOx reduction activity of Cu/SZ, but these authors did not observe a change in the optimum operating temperature window. Further work on the effect of water vapor on NOx reduction over SZ [21,22] showed leaching of sulfate during reaction in the presence of water vapor and Resasco and coworkers [21] reported that this sulfate leaching resulted in a permanent loss in the selectivity of Pd/SZ. Bimetallic palladium catalysts were also investigated for improving NOx reduction activity and hydrothermal stability. Platinum incorporation into Pd/SZ [18,23] and Pd/MOR [24] has been shown to improve both the hydrothermal stability and the catalytic activity. Similar synergistic effects were reported on Co-promoted Pd catalysts supported on MFI [25], MOR [26], ferrierite [27], ZSM-5 [28] and SZ [29]. The improved activity was associated with the activity of the second metal ion in catalyzing NO oxidation to NO_2 in a reaction scheme where Pd ions served as sites for NO_2 reduction [23,28].

Previously, we have reported a novel integrated oxidation/selective catalytic reduction approach to combine three-distinct catalytic functions, namely NOx reduction, CO oxidation and hydrocarbon combustion in a single unit to be utilized for treatment of lean-burn natural gas engine exhaust, without the need for additional fuel injection [30,31]. This approach aims to take advantage of the stronger oxidizing potential of NO_2 relative to NO by utilizing two separate catalytic systems for oxidizing NO to NO_2, and then reducing NO_2 to N_2 with unburned methane available in the lean-burn engine exhaust. NO oxidation to NO_2 is an exothermic and reversible reaction that is thermodynamically limited at high temperatures [32], however, when this reaction takes place in close proximity to a reduction catalyst, NO_2 is removed from the system through SCR reaction, pushing the thermodynamic limitations posed on the system by shifting the equilibrium towards products. The oxidation catalyst also serves to replenish NO_2 that is converted to NO through partial reduction, leading to significantly higher N_2 yields than utilization of an SCR catalyst alone. The oxidation catalyst further takes part in the combustion of excess hydrocarbons and oxidation of carbon monoxide that have not been consumed during the selective catalytic reduction reaction [30]. The dual-catalyst approach has focused on simultaneous development of two separate catalytic systems, which will be physically mixed together. Through this approach, Co-based oxidation catalyst formulations which are able to achieve equilibrium conversions at temperatures as low as 250 °C and gas hour space velocities (GHSV) of 35,000 h^{-1} were developed [33]. Palladium catalysts supported over sulfated zirconia prepared by impregnation of commercial monoclinic zirconia (SZ) support has been reported to give good NO_2 reduction activity with CH_4 around 375–400 °C [34]; however, addition of water vapor to the feed stream resulted in suppression of both NOx reduction and hydrocarbon oxidation activities of the dual-catalyst bed tested under simulated lean exhaust conditions [30]. In a later contribution, we have reported a 'one-pot' sol–gel Pd/SZ catalyst which exhibited significant NO_2 reduction activity around 400–450 °C [35]. As a continuation of our earlier work on dual-catalyst approach for aftertreatment of lean-burn natural gas engine exhaust, in this contribution, we examine the interaction of water vapor with the oxidation and reduction catalyst components of the dual-catalyst scheme, namely Co/ZrO_2 and Pd/SZ, and its implications on the activity and hydrothermal stability of a dual-catalyst bed comprised of these catalysts.

2. Experimental

2.1. Catalyst preparation and characterization

NOx reduction catalyst component (0.3% Pd/SZ) was prepared using a single-step sol–gel procedure which was described in detail earlier [35]. The procedure uses acetic acid as a controlled hydrolysis agent to slow down hydrolysis of zirconium and promote anchoring of sulfur into the zirconium network. Palladium acetate (Aldrich), zirconium propoxide (70% solution in n-propanol, Aldrich) and sulfuric acid (Fisher Sci.) were used as the precursors. A calculated amount of palladium acetate, to give 0.3% Pd loading in the final catalyst, is dissolved in n-propanol and calculated amounts of zirconium propoxide and sulfuric acid were added under constant stirring to achieve final concentrations of 1 M and 0.5 M, respectively. After 30 min of stirring, acetic acid in the amount to give a hydrolysis ratio of 4 is added using a syringe pump, set to deliver 0.2 ml/min of acetic acid. Gelation occurred during the course of 1 h and the gel was dried overnight in a convection oven at 110 °C. The dried gel was ground and calcined at 700 °C for 4 h under continuous flow of oxygen and then, ground to a fine powder before being transferred into vials for storage.

The NO oxidation catalyst (10% Co/ZrO_2) was prepared through an incipient wetness impregnation route using commercial monoclinic zirconia (m-ZrO_2) supplied by Saint-Gobain. The support material, which was received in pelletized form, was ground and sieved to save the 100/150 mesh cut (0.149–0.105 mm). The support was then calcined in air for 3 h at 500 °C. Cobalt nitrate hexahydrate (Aldrich) was used as the precursor. A calculated amount of cobalt precursor to yield 10% loading was dissolved in water and m-ZrO_2 support was impregnated with this solution in two steps. After each impregnation, the catalyst was dried at 110 °C overnight. After the second drying, the catalysts were calcined in air at 500 °C for 3 h. The oxidation catalyst used in this study have been characterized using BET surface area measurements, temperature-programmed techniques, X-ray photoelectron spectroscopy (XPS), X-ray diffraction (XRD), laser Raman spectroscopy and diffuse reflectance Fourier transform infrared spectroscopy (DRIFTS) and the characterization results have been reported previously [33].

Surface area and pore volume measurements were done on a Micromeritics ASAP 2010 accelerated surface area and porosimetry instrument, using nitrogen adsorption/desorption isotherms collected at liquid nitrogen temperature. BJH pore size distributions (PSD) were determined using the desorption branch of the isotherm. Before measurement, samples were degassed overnight at 130 °C under a vacuum of 3 μmHg. Nitrogen physisorption measurements indicate a BET surface area of 67 m^2/g for Pd/SZ and the BJH pore size distribution calculations are in line with that of a mesoporous material with pore size distribution centered at 4 nm.

The chemical states of zirconium, sulfur and oxygen in Pd/SZ were investigated on a Kratos AXIS Ultra X-ray photoelectron spectrometer, using monochromatized Al Kα (1486.7 eV) X-ray source operated at 13 kV and 10 mA. Sample was supported on a double-sided carbon tape for analysis. For studying the variation of sulfur concentration with information depth, spectra were collected before and after etching the surface with 3 kV Ar^+ ion beam for 3 minutes in two cycles, to remove several layers from the surface at a time. X-ray photoelectron spectrum of Pd/SZ was collected in the Zr 3d, S 2p, O 1s and C 1s regions. Collected data were corrected for charge shifting using standard C 1s binding energy of 284.5 eV. Data analysis with background subtraction and curve fitting was done on XPS Peak 4.1. For quantitative comparison of the variation of surface composition with the removal of surface layers,

XPS peak areas of each species were corrected with the respective instrumental atomic sensitivity factors.

2.2. Catalytic activity testing

Steady-state catalytic activity measurements were made within the range of 250–600 °C in a fixed bed, 1/4 in OD stainless steel reactor operating at ambient pressure. Catalyst samples were packed by using quartz wool plugs and the temperature of the catalyst bed was measured and controlled by a K-type thermocouple in contact with the upstream side of the catalyst bed and an Omega 76000 temperature controller. Reactant gases were purchased from Praxair and gas flow rates were controlled using Brooks 5850E mass flow controllers connected to Brooks 0154 electronics control boxes. Reactor effluents were monitored using an online microGC (Varian, CP4900), equipped with molecular sieve 5A and PoraPLOT columns and a chemiluminescence $NO/NO_2/NOx$ analyzer (Thermo Environmental, 42iHL). Reported reactant conversions and N_2 yields are defined as follows:

$$\%\ \text{conversion of } i = \left(\frac{\text{moles of } i \text{ in} - \text{moles of } i \text{ out}}{\text{moles of } i \text{ in}}\right) \times 100$$

$$N_2\ \text{yield} = \left(\frac{2 \times (\text{moles of } N_2 \text{ produced})}{\text{moles of } NO_x \text{ in}}\right) \times 100$$

All carbon and nitrogen balances were always higher than 97%.

Reaction experiments were performed on the dual-catalyst bed as well as on samples of the individual reduction and oxidation catalyst components. In testing the two-catalyst system, samples of the oxidation and reduction catalysts were thoroughly mixed through rigorous shaking in a vial before being placed into the reactor. In order to compare the reduction efficiency, a constant mass of reduction catalyst was used during the NO/NO_2 reduction and dual-catalyst bed experiments, while the amount of the oxidation catalyst was varied. The samples were mixed with 100/150 mesh cut quartz powder to keep the bed volume constant during reactions where oxidation catalyst content was varied. Prior to each reaction experiment the catalyst bed was pretreated in 10% O_2/He (45 sccm) at 400 °C for 30 min followed by cooling/heating to the desired reaction temperature under the same atmosphere. Initial catalytic activity tests were performed using 1000 ppm NO (or NO_2), 3000 ppm CH_4, and 10% O_2 in balance He, with 0–7% H_2O at a GHSV of 20,000 h^{-1}. For all the experiments with the simulated lean exhaust, the feed contained 400 ppm NO, 1700 ppm CH_4, 200 ppm, 100 ppm C_3H_8, 600 ppm CO, 6% CO_2, 10% O_2 and 0–7% H_2O in helium at a GHSV of 20,000 h^{-1}. Water vapor was supplied to the system through a bubbler heated to the desired temperature. The gas lines in contact with water vapor-containing feed was heated during the experiments to prevent condensation.

The stability of the catalytic activity of the dual-catalyst bed was tested during simulated lean exhaust treatment with water vapor-free and water vapor-containing feed streams at 500 °C for 40 h-on-steam. The same experimental set-up as described above for catalytic activity testing was used for the time-on-stream studies. The dual-catalyst bed tested for long term stability under reaction conditions was composed of 25 mg of oxidation catalyst component (Co/ZrO_2) and 200 mg of reduction catalyst component (Pd/SZ).

The reversibility of the effect of water vapor on NO and NO_2 reduction with CH_4 over the reduction catalyst and dual-catalyst bed, simulated lean exhaust treatment and CH_4 oxidation over the dual-catalyst bed and NO oxidation over the oxidation catalyst was investigated by cycling between water vapor-free and wet feeds at steady-state. During these water vapor-free/wet feed cycling experiments, water vapor-free feed stream was first introduced to the reactor and allowed to stabilize for 1 hour. The feed stream was then replaced with 7% H_2O vapor-containing stream, keeping the concentrations of the other components in the feed stream and the total flow rate constant. The process was repeated for three cycles to observe the ability of the system to recover from the effect of water vapor upon recurring exposure.

2.3. Temperature-programmed characterization

Temperature-programmed desorption (TPD) experiments were performed on an automated chemisorption analyzer (Autochem 2910, Micromeritics) connected to an online mass spectrometer (Cirrus II, MKS Instruments, 1–300 amu). For each run, 150 mg of catalyst sample was packed inside a 1/4″ quartz U-tube reactor using quartz wool plugs. For experiments involving water vapor, water vapor was supplied to the reactor by flowing helium through a temperature-controlled, heated bubbler containing deionized water. Prior to each experiment, the water containing bubbler was sonicated for 30 min and then, helium was bubbled through it for one hour to remove dissolved oxygen that water might contain.

Interaction of water vapor with Pd/SZ and Co/ZrO_2 was studied with temperature-programmed desorption following adsorption of water vapor at 35 °C. The samples were calcined *in situ* at 400 °C for 30 min under 10% O_2 in He (45 sccm) and cooled down to 35 °C under the same atmosphere. Then, 1.5% H_2O in He (45 sccm) was introduced to the reactor at 35 °C and adsorption was carried out for 30 min at the same temperature. After purging with He (45 sccm) for at least 30 min, the temperature was ramped at 10 °C/min to 750 °C and the sample was kept at 750 °C for 15 min before cooling.

The effect of water vapor on the interaction of NO, NO_2, N_2O and CH_4 with Pd/SZ was studied through TPD experiments. Both single component (NO, NO_2, N_2O or CH_4) and co-adsorption ($NO–H_2O$, $NO_2–H_2O$, $N_2O–H_2O$ or $CH_4–H_2O$) experiments were carried out. Following *in situ* pretreatment with 10% O_2/He through the above-mentioned procedure, adsorption was carried out at 45 °C for an hour with 1000 ppm NO, NO_2 or N_2O in He or 1% CH_4 in He at a total flow rate of 50 sccm. For co-adsorption studies, 5% water vapor was introduced to the feed stream while keeping the concentration of the other component constant. Following adsorption (or co-adsorption), the reactor was flushed with He (50 sccm) for another 30 min at 45 °C. Then, 5% O_2/He (50 sccm) was introduced to the reactor and the mass signal traces were allowed to stabilize before starting a temperature program from 45 °C to 750 °C at a rate of 10 °C/min. During the temperature-programmed characterization experiments, evolution of species from the surface was monitored with an online mass spectrometer.

2.4. Diffuse reflectance infrared Fourier transform spectroscopy

The interaction of water with the surface of the Pd/SZ was studied with diffuse reflectance infrared Fourier transform spectroscopy (DRIFTS) using a Thermo Nicolet 6700 FT-IR spectrometer equipped with a Ge-on-KBr beamsplitter and a high sensitivity liquid N_2 cooled MCT detector. Water vapor was supplied by bubbling helium through a bubbler kept at room temperature. A sample of 0.3% Pd/SZ, contained in a heated sample cup, was placed in a diffuse reflectance cell, equipped with ZnSe windows. The sample was calcined *in situ* at 400 °C in 10% O_2 in He (30 sccm) for 30 minutes. The temperature was then raised to 600 °C under the same oxygen flow and background spectra were collected every 50 °C, down to 50 °C. At 50 °C, the chamber was flushed with He (30 sccm) for 30 minutes and then, the catalyst was exposed to a stream containing 1.5% H_2O for another 30 min. Following water adsorption,

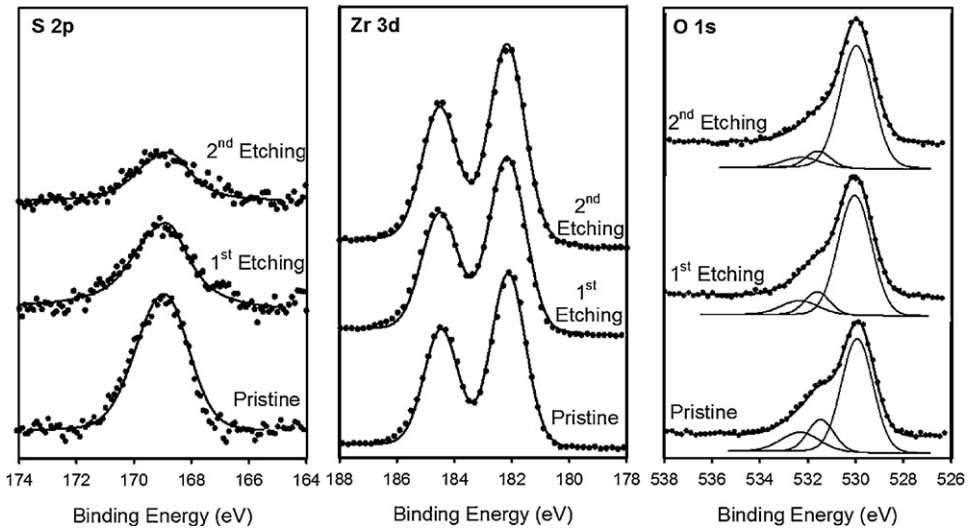

Fig. 1. X-ray photoelectron spectra in the S 2p, Z 3d and O 1s regions of Pd/SZ before and after surface etching.

the cell was again flushed with He for 30 min. Spectra were then collected under He in 50 °C increments up to 600 °C by averaging over 500 scans in the mid-IR range (650–4000 cm^{-1}) at a nominal 2 cm^{-1} resolution. The system was allowed to stabilize for 10 min before collection of each IR spectrum.

3. Results and discussion

3.1. Catalyst characterization

X-ray photoelectron spectra of Pd/SZ in Zr 3d, S 2p and O 1s regions were collected on the pristine sample and after removing several monolayers of the surface by sputtering the surface of the sample with Ar ions to study the variation of surface composition with information depth. Sputtering was carried out in two cycles and X-ray photoelectron spectra were collected after each sputtering cycle. The X-ray photoelectron spectra in the S 2p, Zr 3d and O 1s regions before and after surface etching are shown in Fig. 1.

The curve fitting of the X-ray photoelectron spectrum of S 2p region of pristine Pd/SZ suggests that this envelope is composed of a single component located at 168.8 eV which is characteristic of sulfur species in a sulfate environment [36,37]. The splitting between $2p_{3/2}$ and $2p_{1/2}$ was not observed for the S 2p envelope due to close spin orbit splitting for sulfur and low counts in this region arising from the low intrinsic atomic sensitivity factor for this atom. The curve fitting of Zr 3d doublet of the pristine sample suggested the presence of a single component located at 182.3 eV with a $3d_{5/2}$–$3d_{3/2}$ spin orbit splitting of 2.4 eV, which is in good agreement with values reported in the literature for Zr(IV) in oxides [37]. Etching the surface did not result in shifts in the photopeak locations for Zr 3d and S 2p envelopes and both of the envelopes were composed of single components located at 182.3 eV and 168.8 eV, respectively. The S/Zr atomic ratios before and after sputtering were calculated by using the areas under the photopeaks and instrumental atomic sensitivity factors. Table 1 presents the variation of S/Zr atomic ratio with surface etching. The intensity of the S 2p envelope decreased significantly with etching while no significant change was observed in Zr 3d region. As a result, the calculated S/Zr atomic ratios decrease with etching. This trend in S/Zr atomic ratio is in line with literature [38,39] and suggests the segregation of sulfur species to the top few atomic layers on the surface which is removed by sputtering. During catalyst synthesis the amounts of S and Zr precursors were adjusted such that the S/Zr ratio in the gel was 0.5. A comparison of this theoretical S/Zr ratio with the S/Zr atomic ratio obtained through XPS on the pristine sample suggests a sulfur retention of 20% after the drying and calcination steps. Considering that sulfur concentration decreases from catalyst surface to the bulk, it is reasonable to assume lower than 20% overall sulfur retention on the catalyst.

O 1s envelope was observed as a broad band with a pronounced shoulder at higher binding energies (Fig. 1). The curve fitting of this envelope suggested the presence of three components located at 530 eV, 531.5 eV and 532.3 eV. Table 1 shows the relative contributions of these components to O 1s envelope. The former component located at 530 eV has the largest contribution to the O 1s envelope and its relative contribution to the O 1s envelope increases after etching. This band is characteristic of O^{2-} in metal oxides, i.e., it has been assigned to O^{2-} in zirconia environment. The latter two components were associated with O in sulfate and chemisorbed oxygen (and/or hydroxyl groups), respectively [40,41]. After surface etching, the relative contribution of the latter two species to the O 1s envelope decreased (Table 1). Table 1 also shows the ratio of O 1s component associated with sulfate species (531.5 eV) to the S 2p region calculated using respective instrumental atomic sensitivity factors. This ratio was calculated to be approximately 4 for the pristine and etched samples showing that the sulfate groups retained SO_4^{2-} stoichiometry throughout the surface layers.

Table 1
XPS analysis of Pd/SZ before and after Ar ion sputtering.

	O 1s			O 1s (531.5 eV)/S2p	S 2p/Zr 3d
	530 eV	531.5 eV	532.3 eV		
Pristine	69.8	16.2	14.0	3.94	0.10
1st etching	78.8	11.1	10.0	4.08	0.06
2nd etching	84.2	8.1	7.7	4.04	0.04

3.2. Activity testing

In our earlier papers, we have reported catalyst development studies and activity testing results for a dual-catalyst scheme utilizing a NO oxidation catalyst component and a NOx reduction catalyst component [30]. A conventional incipient wetness impregnation method, where commercial monoclinic ZrO_2 was used as the support, has been pursued for the development of both of the catalyst components and the results on the catalytic activity of these individual components have been published elsewhere [33,34]. We have also reported a 'one-pot' sol–gel technique as an effective method for preparing active Pd/SZ catalysts for NOx reduction and have investigated the effect of palladium loading and calcination temperature on the catalytic activity of these catalysts [35].

Fig. 2a shows a comparison of N_2 yields as a function of temperature during NO_2 and direct NO reduction with CH_4 over a "one-pot" sol–gel Pd/SZ catalyst and NO reduction over a dual-catalyst bed containing the same Pd/SZ catalyst as the CH_4–SCR catalyst component and Co/ZrO_2 as the oxidation catalyst component in a ratio of 4:1. The volcano shaped N_2 yield curve, going through a maximum between 400 °C and 500 °C depending on the composition of the feed and catalyst bed, is typical for SCR reactions carried out under lean conditions. This behavior arises from increased consumption of the reducing agent through combustion with increasing temperature, and thus decreasing its availability for NOx reduction. Fig. 2a shows that, during NO_2 reduction over Pd/SZ, significantly higher N_2 yields than direct NO reduction over the same catalyst were achieved, especially in the low temperature region. This increase in the N_2 yields shows that NO_2 is a more-easily-reduced species than NO and thus, it is more effective than NO in competing with O_2 for the reducing agent. Over a dual-catalyst bed of Pd/SZ and Co/ZrO_2 in a 4-to-1 ratio, N_2 yields that are on the average 12% higher than those achieved during direct NO reduction over Pd/SZ were achieved in the whole temperature range. This behavior is in line with our previous observations on incipient wetness-impregnated catalysts [30]. Increased N_2 yields during dual-catalyst NO reduction results from *in situ* generation of NO_2 which is thought to be an intermediate of NO reduction in some systems [42,43] via the inclusion of an oxidation catalyst component. This allows the reaction network to be catalyzed in a controlled manner, leading to higher N_2 yields than utilization of an SCR catalyst alone. Removal of NO_2 through selective catalytic reduction over the reduction catalyst component enables NO oxidation, which is a reversible reaction that is thermodynamically limited at high temperatures, to proceed at a higher rate. Another important observation that needs to be highlighted is that N_2 yields for dual-catalyst NO reduction continued to increase above those for NO_2 reduction over Pd/SZ alone reaching a maximum of 77% at 500 °C. This behavior is associated with the incorporation of the NO oxidation catalyst component into the dual-catalyst bed. The maximum in the N_2 yield during NO_2 reduction over Pd/SZ corresponds to complete NO_2 conversion, with the major products being N_2 and NO. Incorporation of an NO oxidation catalyst in the dual-catalyst scheme also serves to replenish NO_2 that is converted to NO through partial reduction.

Fig. 2b shows the CH_4 conversions as a function of reaction temperature during the same NOx reduction experiments. Increase in the CH_4 conversions were observed above 400 °C with the inclusion of the oxidation catalyst component in the catalyst bed which shows that the dual-catalyst bed is capable of performing another distinct catalytic function, i.e., oxidation of the unburned hydrocarbon. However, it should be noted that, although the oxidation catalyst can help eliminate unburned hydrocarbons from the exhaust stream, depletion of the reducing agent through combustion with oxygen that is in excess would taper the efficiency of the dual-catalyst system. Therefore, the effect of the relative contributions of the oxidation and reduction catalysts to the overall activity was studied by changing the amount of oxidation catalyst component while keeping the amount of reduction catalyst component constant. The tested oxidation-to-reduction catalyst ratios were 1:8, 1:4; 1:2 and 1:1. Fig. 2c shows N_2 yields achieved at 500 °C during NO reduction over these dual-catalyst beds. Note that, incorporating different amounts of oxidation catalyst to the dual-catalyst bed did not change the window of operation of the system. As shown in the figure, incorporation of small amounts of oxidation catalyst to the reduction catalyst results in improved N_2 yields while further increase in the amount of oxidation catalyst suppressed it. Interestingly, the dual-catalyst bed containing oxidation-to-reduction catalysts in a ratio of 1:1 was not capable of achieving a N_2 yields equivalent to what were observed over Pd/SZ, as CH_4 combustion over the oxidation catalyst dominates

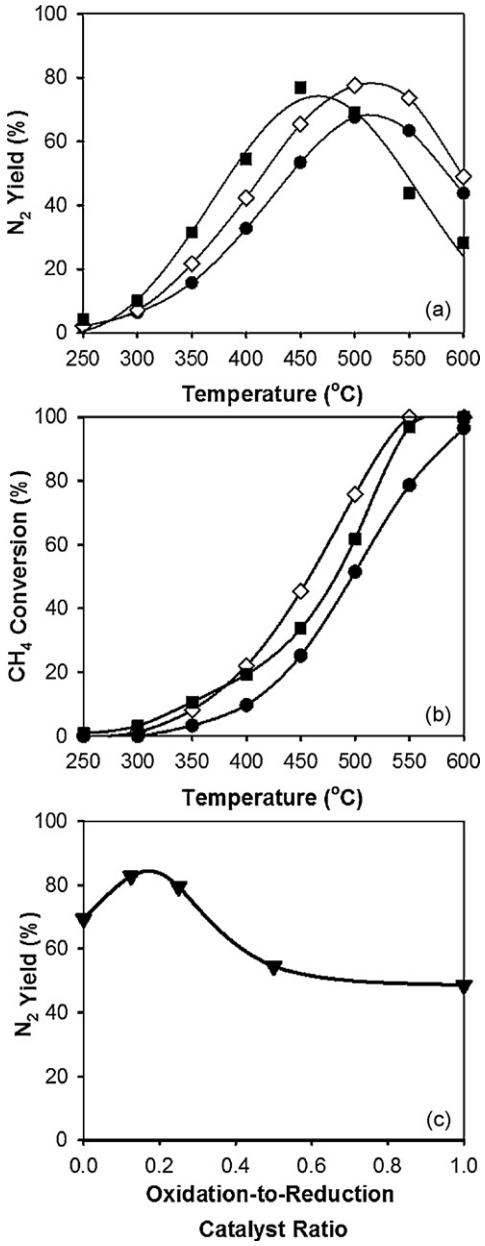

Fig. 2. Comparison of (a) N_2 yields and (b) CH_4 conversions during of NO (●) and NO_2 (■) reduction over Pd/SZ, and NO (◊) reduction over Pd/SZ–Co/ZrO_2 dual-catalyst bed in a 4:1 ratio and (c) N_2 yield at 500 °C as a function of oxidation-to-reduction catalyst ratio. *Reaction conditions:* [NO] (or [NO_2]) = 1000 ppm, [CH_4] = 3000 ppm, [O_2] = 10% in He; 1 atm; GHSV = 20,000 h^{-1}.

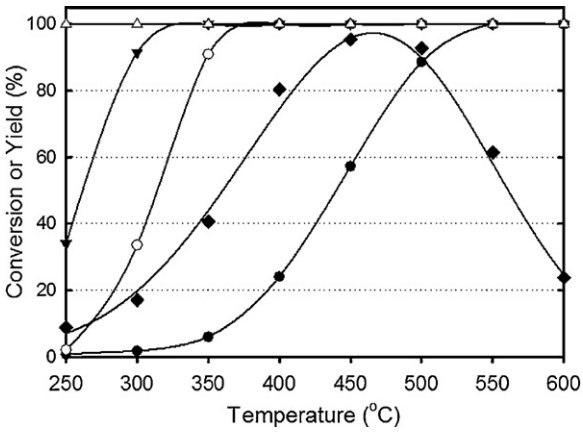

Fig. 3. N_2 (♦) yields and, CO (△), CH_4 (●), C_2H_6 (○) and C_3H_8 (▼) conversions during simulated lean exhaust treatment over a dual-catalyst bed of Co/ZrO_2 and Pd/SZ in a 1:8 ratio. *Reaction conditions:* [NO] = 400 ppm, [CH_4] = 1700 ppm, [C_2H_6] = 200 ppm, [C_3H_8] = 100 ppm, [CO] = 600 ppm, [CO_2] = 6%, [O_2] = 10% in He; 1 atm; GHSV = 20,000 h^{-1}.

over selective catalytic reduction. The composition of the best performing catalyst bed consisting of Co/ZrO_2 and sol–gel Pd/SZ is different than what we reported for incipient wetness impregnation catalysts [30] and demonstrates that optimization studies on the contribution of the two catalytic functions to dual-catalyst scheme is of crucial importance to fully exploit its benefits.

The activity of the best performing mixed bed of oxidation and reduction catalysts was further tested with simulated lean exhaust. Fig. 3 shows steady-state N_2 yield and CH_4, C_2H_6, C_3H_8 and CO conversions as a function of temperature in 250–600 °C range. During simulated lean exhaust treatment with the dual-catalyst system, N_2 yield went through a maximum around 450–500 °C, achieving yields in excess of 95% showing that the SCR activity was not affected by the presence of other oxidizing and reducing agents. In this broad operating window, complete conversion of C_2H_6, C_3H_8 and CO, and significant conversion of CH_4 (~80%), was achieved. In fact, the dual-catalyst system was capable of achieving complete C_2H_6 and C_3H_8 conversions around 300 °C and 350 °C, respectively. Complete conversion of CO was achieved at temperatures as low as 250 °C over the dual-catalyst bed which could be associated with the presence of the oxidation catalyst component in the catalyst bed, as Co/ZrO_2 is also known to be an active catalyst for low temperature CO oxidation and preferential CO oxidation [44,45]. Control experiments by eliminating either CO or C_2H_6 and C_3H_8 from the feed stream were performed in order to elucidate whether these components contribute to the NOx reduction activity over the dual-catalyst system, especially at temperatures where CH_4 activation over the reduction catalyst component does not take place at a considerable rate. Elimination of CO from the feed stream resulted in an average decrease of 11% in the N_2 yield in 250–450 °C region (not shown) suggesting that CO is either directly involved in NOx reduction or promotes HC–SCR over Pd/SZ. It is also plausible that the heat released during CO oxidation could increase the surface temperature resulting in higher rates for NOx reduction in the presence of CO. However, the calculations assuming adiabatic conditions showed that the temperature increase due to the heat released from CO oxidation was insignificant when compared to the reaction temperatures. The effect diminished with increasing temperature, which might be associated with increased rate of CO consumption through reaction with oxygen with increasing temperature rendering CO unavailable for NOx reduction. Elimination of C_2H_6 and C_3H_8 from the feed stream did not result in a significant change in the N_2 yields across the whole temperature range (not shown).

3.3. Effect of water vapor on NO_2 reduction over Pd/SZ

The investigation of the effect of water vapor on the activity and stability of catalytic SCR systems is of crucial importance as water is not only a product of both SCR and CH_4 combustion in the aftertreatment system, but it also exists in significant proportions in the engine exhausts. Our previous investigations on the effect of water vapor on NO oxidation over Co/ZrO_2 through steady-state reaction experiments has shown that this catalyst is capable of achieving equilibrium conversion of 90% at about 250 °C in the presence of 10% water vapor at a GHSV of 35,000 h^{-1} [33]. Furthermore, studies on reversibility of the effect of water vapor through cycling between feed streams with and without water during NO oxidation showed that this catalyst was able to keep the same level of activity in both cases. These results will be presented in Section 3.4. A negative effect of water vapor was observed on the NOx reduction activity of the dual-catalyst mixed bed and the effect was speculated to be associated with competitive adsorption taking place over the reduction catalyst component [30]. To further investigate this phenomenon, NO_2 reduction activity of the Pd/SZ prepared by a sol–gel technique was tested in the presence of 1.5–7% water vapor in the feed stream through steady-state reaction experiments. Fig. 4 shows the effect of water vapor on NO_2 and CH_4 conversions and product yields as a function of water vapor concentration and temperature during NO_2 reduction with CH_4 over Pd/SZ. Presence of water vapor in the feed significantly suppressed NO_2 conversion below 450 °C. The light-off for NO_2 conversion under water vapor-free conditions occurs at 317 °C. In the presence of 1.5% water vapor the light-off temperature shifted by 50–370 °C and, further increasing the water vapor content to 7% shifted the light-off temperature to 410 °C. Complete conversion of NO_2 was observed regardless of the water vapor content of the feed stream, although the temperature at which complete conversion was achieved shifted to higher temperatures with increasing water vapor content. At 450 °C where highest NOx reduction activity was observed over the dual-catalyst bed, NO_2 conversion was independent of water vapor concentration. Fig. 4b shows N_2 yields from the above-mentioned three experiments. The maximum N_2 yield decreased from 73% under water vapor-free conditions to 62% in the presence of 1.5% water vapor along with a shift in the temperature window where the maximum N_2 yield was obtained. When 7% water vapor is present, the N_2 yield further decreased and 54% N_2 yield was achieved with further shift of the optimum operating window to slightly above 500 °C. Above 500 °C, the effect of water vapor on NO_2 reduction activity diminishes as the consumption of the reducing agent through combustion takes off and the availability of the reducing agent for SCR rather than possible competition from water for active sites becomes the limiting factor for NOx reduction. Another possible reason as to why the catalytic activity is independent of the water content of the feed stream at temperatures above 500 °C is the decreased abundance of water ad-species over the surface at the temperatures under consideration. Temperature-programmed water desorption studies, which will be discussed later, showed that the desorption of a significant portion of adsorbed water takes place below 500 °C; therefore, it is plausible that at these temperatures water is not able to compete with reactants/intermediates for the active sites.

Fig. 4c and d shows the NO and N_2 yields for the above-mentioned NO_2 reduction experiments. The change in NO yield as a function of temperature evidences the presence of three different temperature regions where different reactions in the reaction network dominate. The initial increase in the NO yield is associated with partial reduction of NO_2 where NO is not activated for SCR in the temperature region under consideration. The maximum of the NO yield curve roughly corresponds to the tem-

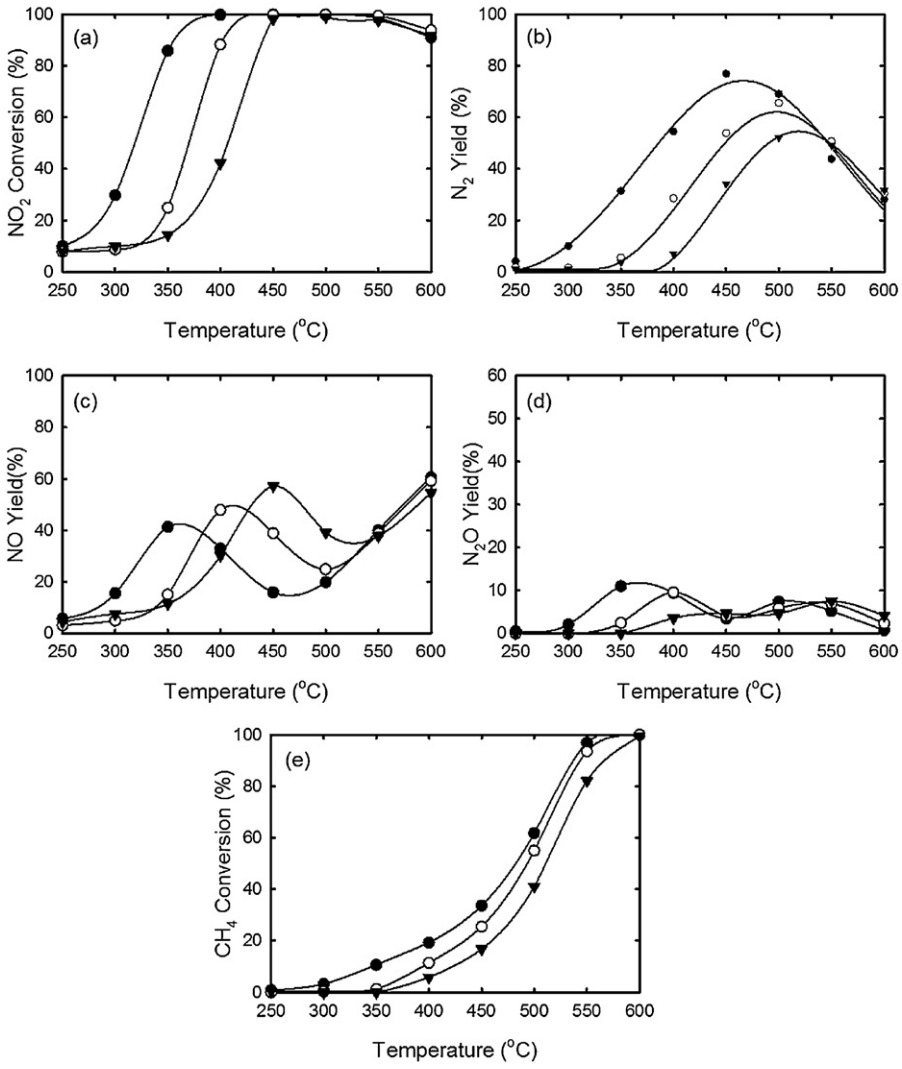

Fig. 4. Effect of water vapor on NO_2 reduction over Pd/SZ. *Reaction conditions:* $[NO_2] = 1000$ ppm, $[CH_4] = 3000$ ppm, $[O_2] = 10\%$ and $[H_2O] = 0\%$ (●), 1.5% (○) or 7% (▼) in He; 1 atm; GHSV = 20,000 h^{-1}.

perature where complete conversion of NO_2 is observed. In the second temperature region, NO yield starts to decrease which is accompanied with increasing N_2 yield and shows that NO reduction over Pd/SZ takes off. NO yield continues to decrease and goes through a minimum before starting to increase again. This minimum corresponds to the onset of the third region. In this region, NO yield increases as NO is the thermodynamically favored product of NO-NO_2 oxidation/reduction equilibrium and this results in NO build up since the rate of NO conversion through SCR is slow due to the limited availability of the reducing agent which is consumed through combustion with excess oxygen.

For the water vapor-free feed, NO yield increases up to 350 °C and starts to decrease as NO reduction starts to take off going through a minimum at 460 °C. The second region, where selective catalytic reduction dominates in the reaction network, shifts to higher temperatures with increasing water content of the feed stream. Furthermore, with increasing water vapor content, NO yield increases at the expense of N_2 yield in this region, such that, NO yields of 58%, 40% and 19% and N_2 yields of 37%, 55% and 75% were achieved in the presence of 7%, 1.5% and 0% water vapor, respectively, at 450 °C, where the maximum NOx reduction activity was achieved over the dual-catalyst bed. These results suggest that presence of water vapor reduces the NOx reduction activity of Pd/SZ and increases NO yield, possibly through blocking the sites for NO adsorption/reduction. Similar to N_2 yield, presence of water vapor in the feed stream does not have any effect on the NO yield above 500 °C as availability of the reducing agent, rather than competition from water tends to be rate limiting. Fig. 4d shows that, the presence of water vapor also inhibits the formation of N_2O, which is an undesirable side product of NOx reduction reaction. A maximum of 13% N_2O yield is observed at 350 °C under water vapor-free conditions. N_2O yield decreases to 10% in the presence of 1.5% water and the temperature window where maximum N_2O yield is observed shifts to higher temperatures. Fig. 4e shows the methane conversions during these three experiments. Light-off for methane occurs at 460 °C under water vapor-free conditions and shifts to 490 °C in the presence of 1.5% water vapor further shifting to 520 °C with 7% water vapor present in the feed stream.

3.4. Reversibility of the effect of water vapor

The reversibility of the effect of water vapor on NO_2 reduction, NO oxidation and CH_4 oxidation was studied by periodically cycling between streams containing 0% or 7% water vapor. During these experiments, water vapor-free feed stream was introduced to the reactor and the system was allowed to reach steady-state.

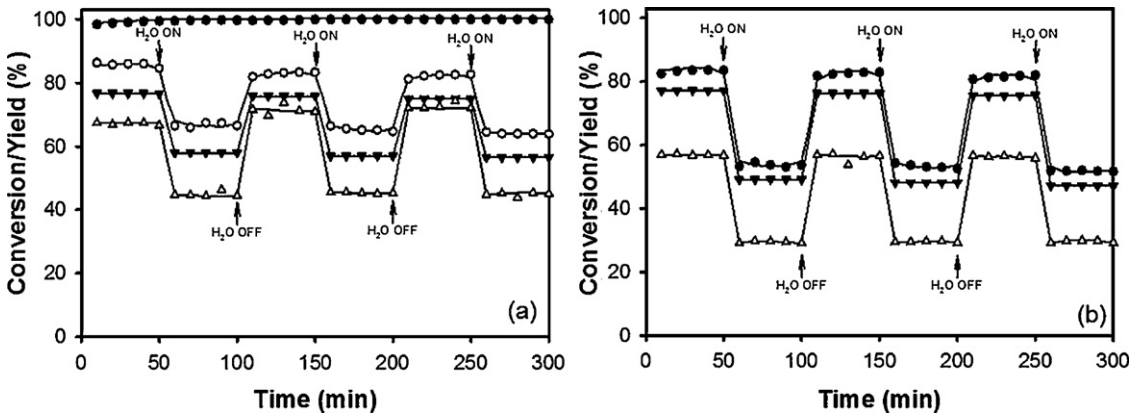

Fig. 5. Reversibility of the effect of water vapor on NO/NO_2 (●), NOx (○), CH_4 (△) conversions and N_2 yields (▼) during (a) NO_2 reduction with CH_4 over Pd/SZ and (b) direct NO reduction with CH_4 over Pd/SZ. *Reaction conditions:* 500 °C; 1 atm; GHSV = 20,000 h^{-1}; [NO] (or [NO_2]) = 1000 ppm, [CH_4] = 3000 ppm, [O_2] = 10% and [H_2O] = 0% or 7% in He.

When steady-state is reached, water vapor was introduced to the system while keeping the total flow rate through the reactor and concentrations of the reactants constant. During each of the experiments, the water vapor-free–wet feed cycling was repeated for three cycles to observe the response/recovery of the catalyst upon repeated exposure to water vapor.

Fig. 5 shows NO (or NO_2), total NOx ($NO + NO_2$) and CH_4 conversions, and N_2 yields for feed cycling experiments during NO and NO_2 reduction over Pd/SZ. For all of the experiments, presence of water vapor in the feed was observed to have a negative effect on the NOx reduction activity, decreasing NOx conversion and N_2 yield in varying amounts, but the activity recovered completely upon removal of water vapor. Fig. 5a shows NO_2 and total NOx conversions during NO_2 reduction over Pd/SZ. During the first water vapor-free feed cycle, complete conversion of NO_2 and 86% total NOx conversion were achieved. Upon introduction of water vapor-containing feed stream, total NOx conversion decreased to 67%. The N_2 yield also followed a similar trend and decreased from 78% to 64%. These results imply a change in the reaction product distribution in favor of NO and suggest that water vapor suppresses N_2 formation while resulting in increased NO yields. Upon removal of water vapor from the feed immediate recovery of the NOx reduction activity was observed. Recurring exposure to water vapor-free feed–wet feed cycles showed that the effect of water vapor on NOx reduction was completely reversible.

Fig. 5b shows NOx/NO conversion and N_2 yields for a similar experiment involving direct NO reduction over Pd/SZ. Under water vapor-free feed stream, steady-state NO and NOx conversions were 82%, and the N_2 yield was 77%. NO and total NOx conversions followed each other closely during the experiment showing that NO oxidation did not take place under these reaction conditions to any measurable extent or any NO_2 that might have been formed was further reacted rapidly. With the introduction of water vapor-containing feed stream, NO/NOx conversions decreased to 53% and similarly, N_2 yield decreased to 49%. Similar to the feed cycling experiment with NO_2, the NO reduction activity recovered immediately upon removal of water vapor from the feed, reaching the pre-water exposure values for both NOx conversion and N_2 yield. A comparison of the magnitudes of change in both NOx conversions and N_2 yields with the introduction of water vapor-containing feed during NO_2 reduction and NO reduction over Pd/SZ shows that the inhibitory effect of water vapor was more pronounced for NO reduction. This result further supports the findings of temperature-programmed desorption experiments discussed in Section 3.6, where water vapor was observed to have no effect on NO_2 adsorption over Pd/SZ while it significantly inhibited adsorption of NO on the surface.

As shown in Fig. 5a and b, introduction of water vapor-containing feed also resulted in a decrease in the CH_4 conversion levels. Inhibitory effect of water vapor on CH_4 conversion over Pd-based catalysts is well documented. Cullis et al. [46] have suggested the formation of $Pd(OH)_2$ which is inactive for CH_4 combustion and further showed that the ability of the support to retain water affected the stability of $Pd(OH)_2$. Burch et al. [47] suggested that release of –OH from $Pd(OH)_2$ rather than C–H bond activation was the rate limiting step in CH_4 combustion. Ribeiro et al. [48] reported negative reaction order with respect to water for methane combustion over palladium catalysts, evidencing the competition between H_2O and CH_4 during CH_4 combustion. Complete recovery of the CH_4 conversion was observed following each water vapor exposure cycle, showing that the inhibitory effect of water vapor is completely reversible.

The same cycling experiment was repeated during both NO reduction and simulated lean exhaust treatment over a dual-catalyst bed of Pd/SZ and Co/ZrO_2 in a ratio of 8:1 (Figs. 6 and 7, respectively). During NO reduction over the dual-catalyst bed, 98% NO and 94% NOx conversions were achieved along with a N_2 yield of 88% at steady-state with water vapor-free feed. Throughout the experiment, NO conversions followed the same trend as total NOx conversions, but were always higher than total NOx conversions, which is due to oxidation of NO over the oxidation catalyst. Upon the introduction of water vapor-containing feed NO and total NOx conversion decreased to 89% and 74%, respectively. Similarly, the N_2

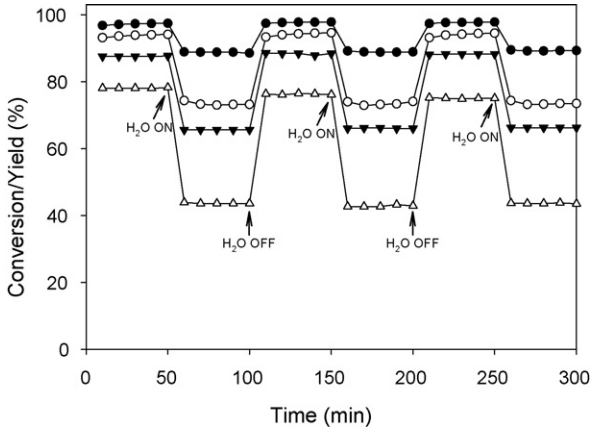

Fig. 6. Reversibility of the effect of water vapor on NO (●), NOx (○), CH_4 (△) conversions and N_2 yields (▼) during NO reduction with CH_4 over a mixed bed of Co/ZrO_2 and Pd/SZ in a 1:8 ratio. *Reaction conditions:* 500 °C; 1 atm; GHSV = 20,000 h^{-1}; [NO] = 1000 ppm, [CH_4] = 3000 ppm, [O_2] = 10% and [H_2O] = 0% or 7% in He.

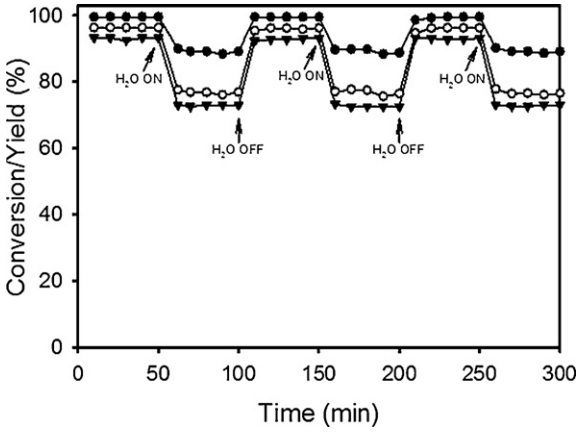

Fig. 7. Reversibility of the effect of water vapor on NO (●), NOx (○), CH_4 (△) conversions and N_2 yields (▼) during simulated lean exhaust treatment over a mixed bed of Co/ZrO_2 and Pd/SZ in a 1:8 ratio. *Reaction conditions*: 500 °C; 1 atm; GHSV = 20,000 h^{-1}; [NO] = 400 ppm, [CH_4] = 1700 ppm, [C_2H_6] = 200 ppm, [C_3H_8] = 100 ppm, [CO] = 600 ppm, [CO_2] = 6%, [O_2] = 10% and [H_2O] = 0% or 7% in He.

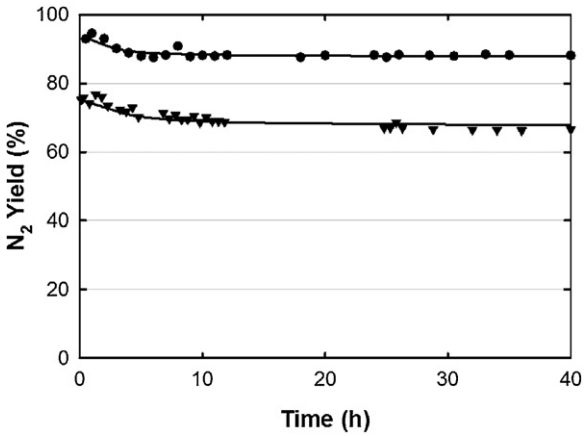

Fig. 9. Stability of a mixed bed of Pd/SZ and Co/ZrO_2 during simulated lean exhaust treatment in the absence (●) and presence (▼) of water vapor. *Reaction conditions:* 500 °C; 1 atm; GHSV = 20,000 h^{-1}; [NO] = 400 ppm, [CH_4] = 1700 ppm, [C_2H_6] = 200 ppm, [C_3H_8] = 100 ppm, [CO] = 600 ppm, [CO_2] = 6%, [O_2] = 10% and [H_2O] = 0% or 7% in He.

yield also decreased to 67%. Interestingly, the decrease in NO/NOx conversions and N_2 yield with the introduction of water is significantly lower for NO reduction over the dual-catalyst bed in comparison to direct NO reduction over Pd/SZ, and shows that the dual-catalyst approach not only enables higher NOx conversions and N_2 yields to be achieved, but also acts to offset the detrimental effect of water vapor on the NO reduction activity of Pd/SZ. Upon removal of water vapor, complete recovery of both NO/NOx conversion and N_2 yield was observed and the steady-state NO/NOx conversion and N_2 yield values did not change with recurring water exposure. Similar observations on the reversibility of the inhibitory effect of water on NO reduction have been reported for Pd–Co/SZ and Pd–Co/ZSM-5 [15,19]. During simulated lean exhaust treatment over a dual-catalyst bed of Pd/SZ and Co/ZrO_2 in an 8:1 ratio, steady-state NO and NOx conversions of 99.5% and 96% was achieved with a N_2 yield of 92% (Fig. 7). With the introduction of water vapor-containing feed stream the NO conversion decreased to 89% while total NOx conversion decreased to 77%. The N_2 yield under these conditions was 72%. The dual-catalyst bed was able to recover from the effect of water vapor upon removal of water vapor from the feed.

A similar water vapor-free–wet feed switch experiment was run over Co/ZrO_2 at 400 °C, to investigate the effect of water vapor on NO oxidation over the oxidation catalyst component. Fig. 8 shows

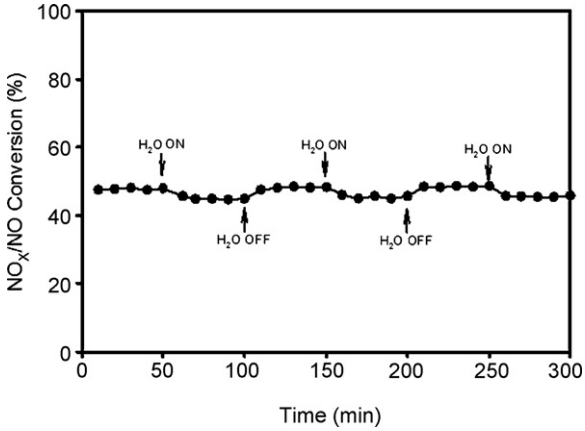

Fig. 8. Reversibility of the effect of water vapor NO oxidation over Co/ZrO_2. *Reaction conditions:* 400 °C; 1 atm; GHSV = 100,000 h^{-1}; [NO] = 1000 ppm, [O_2] = 10% and [H_2O] = 0% or 7% in He.

NO and NOx conversions for NO oxidation over Co/ZrO_2 during an experiment similar to above-mentioned water vapor-free–water vapor-containing feed cycling experiments. The reaction conditions were maintained away from equilibrium during this cycling experiment to assure that the experiment was run in the kinetically controlled regime. As expected, no products of NOx reduction were observed during this experiment. The steady-state NO conversion under water vapor-free feed was 48% which then decreased to 45–46% upon introduction of wet feed under the same conditions. The NO conversion recovered upon removal of water vapor from the feed and recurring exposure of the catalyst to water vapor under reaction conditions did not result in deactivation. These observations are in line with previously reported findings [33] and show that water vapor has no major inhibition effect on NO oxidation over 10% Co/ZrO_2.

Fig. 9 presents the N_2 yield as a function of time-on-stream for a dual-catalyst bed of oxidation-to-reduction catalyst components in a ratio of 1:8 under two different feed compositions, namely, in the absence and presence of water vapor. For the water vapor-free feed condition, the initial nitrogen yield was 95% and decreased to 88% during the first 10 h on stream, where it was stable for the rest of the experiment. A similar trend was observed in the presence of water vapor. Under the feed containing 7% water vapor, an initial N_2 yield of 77% was achieved which decreased to 68% during the first 10 h on-stream, stabilizing at this value for the rest of the experiment. Although lower N_2 yields were achieved in the presence of water vapor, the activity stabilized after the first ten hours on-stream and the dual-catalyst retained stable activity in the presence of water vapor during the 40-h test. The similar behavior of the dual-catalyst system under water vapor-free and water vapor-containing feeds provides further evidence for competitive adsorption related phenomena, where water vapor competes with reactants and/or products resulting in reduced rates of reaction rather than gradual deactivation of the active sites in the presence of water vapor.

The catalytic activity tests carried out in the presence of water vapor show that while water vapor has no significant effect on NO oxidation over the oxidation catalyst component, it affects the NOx reduction activity of Pd/SZ possibly through competitive adsorption with one or more of the reactant species resulting in decreased catalytic activity. Therefore, the interaction of water vapor with Pd/SZ and reactants and its effect on the thermal stability of sulfate groups was further investigated.

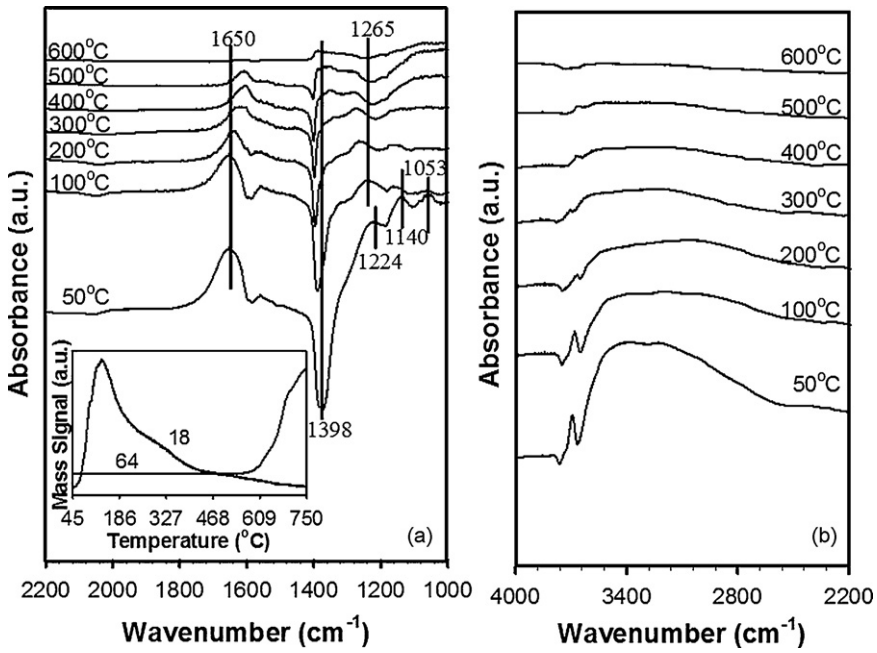

Fig. 10. DRIFT spectra during H_2O-TPD on Pd/SZ (a) low wavenumber region and (b) high wavenumber region. (*Inset*: H_2O ($m/z = 18$) and SO_2 ($m/z = 64$) traces during H_2O-TPD.)

3.5. Interaction of H_2O with Pd/SZ

The interaction of water vapor with Pd/SZ was studied through temperature-programmed desorption studies. During these experiments Pd/SZ surface was saturated with adsorbed water species at 50 °C and the thermal transformation of H_2O and evolution of H_2O from the surface during heating was monitored with mass spectrometry and *in situ* DRIFTS. Following pretreatment in O_2/He, background spectra were collected at each temperature level under O_2/He, similarly, sample spectra were collected under O_2/He. Fig. 10 shows DRIFTS spectra and the H_2O ($m/z = 18$) and SO_4 ($m/z = 64$) traces collected during these experiments (inset). Following H_2O adsorption and He flush at 50 °C, bands at 1650 cm^{-1}, 1398 cm^{-1}, 1224 cm^{-1}, 1140 cm^{-1} and 1053 cm^{-1} were resolved in the low wavenumber region and these were accompanied with a broad band in the high wavenumber region that is centered around 3400 cm^{-1} and another sharp band located at 3695 cm^{-1}. The band at 1650 cm^{-1} is associated with δ_{HOH} modes of molecularly adsorbed water, whereas the broad band at 3400 cm^{-1} can be associated with υ_{OH} modes of surface hydroxyls and physisorbed water [49–51]. With increasing temperature the intensity of both the 3400 cm^{-1} and 1650 cm^{-1} bands decrease, evidencing evolution of water from the surface. The $m/z = 18$ trace (see Fig. 10a – inset) exhibited a sharp water evolution band (T_{max} = 119 °C) at the onset of the temperature program, which can be associated with desorption of physisorbed water. A broad shoulder corresponding to 200–400 °C region was also resolved. The 1650 cm^{-1} band red shifts with temperature which might be associated with decreased coordination of adsorbed water species. A similar shift with dehydration of sulfated zirconia surface has previously been reported [50–52]. Morterra et al. [50,51] suggested appearance of a new band at lower wavenumbers, ca. 1600 cm^{-1}, rather than a red shift of the high wavenumber band and associated the artifact with the formation of $[H_3O]^+$ groups on the surface at early dehydration stages. These species were more stable than H-bonded H_2O on the surface and remained on the surface after treatment at elevated temperatures [52].

The SO_2 ($m/z = 64$) trace collected during the H_2O-TPD does not exhibit any desorption bands that accompany water desorption from the surface. Onset of SO_2 desorption form the surface was observed at 600 °C. The negative band at 1398 cm^{-1} corresponds to $\upsilon_{S=O}$ modes of highly covalent sulfate species that are interacting with water ad-species. The negative peak intensity of the 1398 cm^{-1} band decreases and is accompanied by a blue shift with increasing temperature. The blue shift in this band with increasing temperature suggests an increase in the covalent character of the sulfates, which arises from elimination of protonic moieties with temperature. Bands located at 1053 cm^{-1}, 1140 cm^{-1} and 1224 cm^{-1} were assigned to bidentate SO_4^{2-} [49]. Upon heating the sample to 150 °C, hydration of these species into H_2SO_4 was observed through a band at 1265 cm^{-1}. At 600 °C, the spectrum was essentially free of absorption bands. These results are in line with our previous work [30] and literature findings [49,51] and show that the adsorption of water on to Pd/SZ was a reversible process that did not alter the sulfate groups on the surface.

3.6. Effect of H_2O on the interaction of NO, NO_2 and CH_4 with Pd/SZ

Temperature-programmed desorption (TPD) experiments were carried out following adsorption of NO, NO_2, N_2O and CH_4 to investigate the thermal transformation of these species on the Pd/SZ surface. Similar TPD experiments were also carried out following co-adsorption of water with these species to observe the effect of water vapor on the interaction of these molecules with the catalyst surface. We have previously shown that heat treatment of Pd/SZ under inert atmosphere resulted in loss of higher amount of sulfate species than heat treatment under oxidizing atmosphere and suggested that presence of O_2 stabilized sulfate groups [34] therefore, temperature-programmed desorption of the adsorbed species was carried out under oxidizing atmosphere in order to prevent reduction of surface sulfate species during heating under inert atmosphere.

Fig. 11a shows CH_4 ($m/z = 15$), CO_2 ($m/z = 44$) and SO_2 ($m/z = 64$) traces collected during TPD of methane from Pd/SZ. CH_4 trace exhibits a weak desorption band in 140 - 470 °C region (T_{max} = 230 °C). Pd-based catalysts are well known for their activity in methane combustion reaction [53–55] therefore, almost all of the

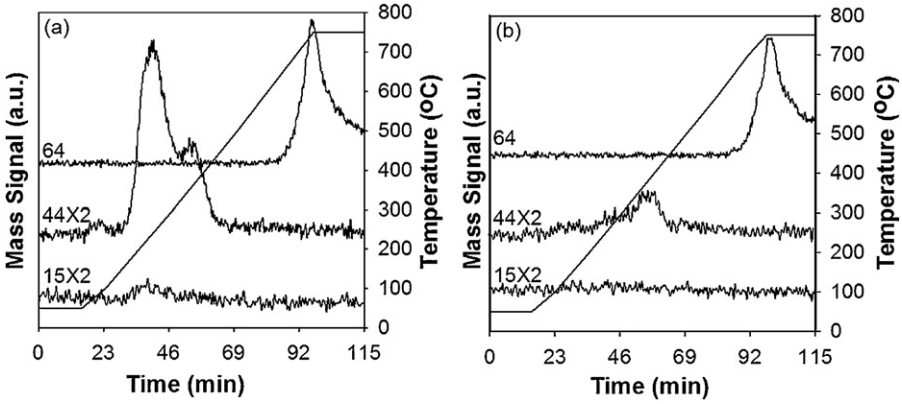

Fig. 11. TPD profiles of CH_4 (m/e = 15), CO_2 (m/e = 44) and SO_2 (m/e = 64) following (a) CH_4 adsorption and (b) CH_4 and H_2O co-adsorption over Pd/SZ at 50 °C.

adsorbed methane species can be expected to desorb as oxidation products under the oxidizing conditions utilized for the TPD. A well-resolved CO_2 desorption band is observed in 144–470 °C region (T_{max} = 230 °C), with a well-defined shoulder with T_{max} = 355 °C. The stability of surface sulfate species was monitored through sulfur dioxide (m/z = 64) trace. Sulfate groups were thermally stable in the presence of gas phase oxygen and no sulfate desorption from the surface is observed to accompany either CH_4 or CO_2 desorption. The onset of a desorption band is observed for sulfur dioxide (m/z = 64) trace at 625 °C. Fig. 11b shows CO_2 (m/z = 44), CH_4 (m/z = 15) and SO_2 (m/z = 64) traces collected during a similar TPD experiment following co-adsorption of water vapor and CH_4 at 50 °C. Co-adsorption of water vapor resulted in significant changes in the CO_2 and CH_4 traces whereas it had no effect on SO_2 trace. Similar to the water vapor-free experiment, SO_2 trace showed no desorption features below 600 °C and desorption took off at 625 °C. The CO_2 trace only exhibited a weak band in 200–460 °C region (T_{max} = 370 °C) which corresponds to the high temperature shoulder observed during TPD following CH_4 adsorption under water vapor-free conditions. However, this desorption feature was much weaker in intensity when compared to the peak observed following adsorption under water vapor-free conditions. Furthermore, no features that could be associated with methane desorption was observed. Evidence suggests that the presence of water vapor competes with methane adsorption rather than suppressing methane oxidation pathways on the surface.

Similar TPD experiments were carried out following NO_2 adsorption and NO_2–H_2O co-adsorption over Pd/SZ. Fig. 12a and b shows comparison of NO_2 (m/z = 46), NO (m/z = 30), N_2O (m/z = 44) and SO_2 (m/z = 64) desorption profiles collected during temperature-programmed desorption following NO_2 adsorption and NO_2–H_2O co-adsorption, respectively. As apparent from the TPD profiles, unlike methane, co-adsorption of water did not affect the interaction of NO_2 with Pd/SZ. In either case, NO_2 desorption from the surface starts with the onset of the temperature program and two desorption features are observed which are located at 125 °C and 336 °C. Significant NO_2 desorption form the surface suggests reversible adsorption of significant amounts of NO_2 on to the surface. Regardless of whether adsorption or co-adsorption was carried out, small amounts of both NO and N_2O were observed. NO_2 and NO profiles closely follow each other. The fragmentation of NO_2 by the mass spectrometer was determined prior to the experiments and the ratio of NO_2 to NO was found to be 1.46:1. The relative intensity of the NO signal is slightly higher than predicted by NO_2 fragmentation, indicating that a small amount of NO_2 decomposes on the catalyst surface. The N_2O profile shows a single, weakly resolved desorption feature which closely corresponds to NO_2 desorption, further suggesting NO_2 dissociation on the surface. The N_2O desorption band is less intense in the case of NO_2-H_2O co-adsorption compared to NO_2 adsorption suggesting that water might be interfering with NO_2 dissociation on the surface although it seems to have no effect on its adsorption on to the surface. Similar to CH_4 adsorption, sulfate groups were stable during the TPD and the onset of SO_2 desorption was not observed until the temperature was raised above 625 °C.

Fig. 13 shows NO (m/z = 30), N_2O (m/z = 44), NO_2 (m/z = 46) and SO_2 (m/z = 64) traces collected during a similar series of experiments involving NO and NO-H_2O adsorption over Pd/SZ. Two well defined desorption features were resolved in the m/z = 30 desorption trace following NO adsorption. The onset of the low temperature band corresponded to the onset of the temperature program and the peak maximum occurred at 100 °C. The high

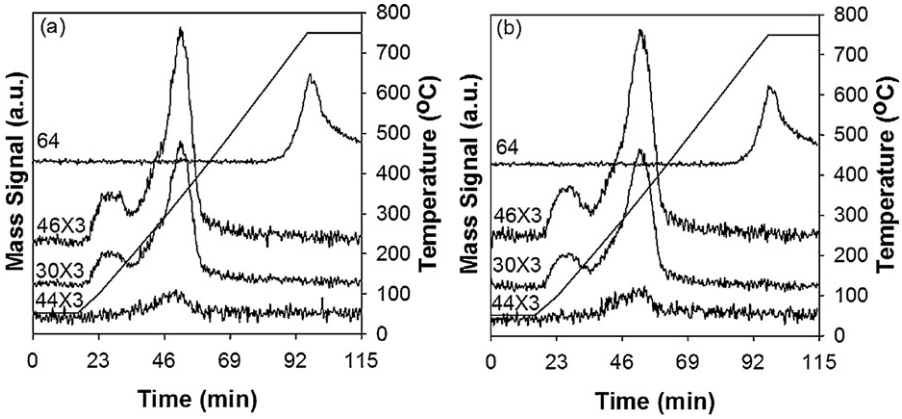

Fig. 12. TPD profiles of NO (m/e = 30), NO_2 (m/e = 46), N_2O (m/e = 44) and SO_2 (m/e = 64) following (a) NO_2 adsorption and (b) NO_2 and H_2O co-adsorption over Pd/SZ at 50 °C.

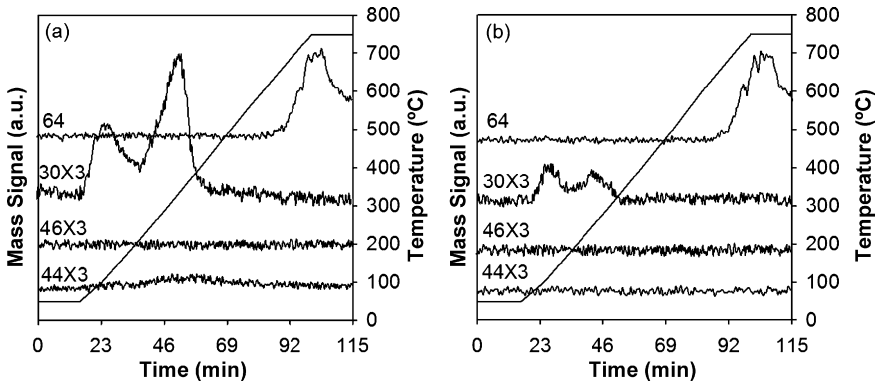

Fig. 13. TPD profiles of NO ($m/e = 30$), NO_2 ($m/e = 46$), N_2O ($m/e = 44$) and SO_2 ($m/e = 64$) following (a) NO adsorption and (b) NO and H_2O co-adsorption over Pd/SZ at 50 °C.

temperature band was observed at T_{max} = 336 °C. Desorption of neither NO_2 nor N_2O was observed in the entire temperature range suggesting that NO did not further react on the catalyst surface. Following co-adsorption of NO and water vapor, two weakly resolved desorption features (T_{max} = 100 °C and 250 °C) were observed in the NO desorption trace. The significant decrease in the intensity of the NO desorption bands suggest that water vapor interacts with the surface to block the sites for adsorption of NO allowing smaller amounts of NO to be retained on the surface. Similar conclusions on H_2O inhibition of NO adsorption on Co/ZSM-5 was also reported by Li et al. [56]. No desorption features that could be associated with further reaction of NO on the surface in the presence of water was observed in the NO_2 and N_2O traces. In either case, sulfur species were observed to be stable under these experimental conditions up to 625 °C, where the onset of an SO_2 desorption feature was resolved.

4. Conclusions

The activity and hydrothermal stability of Pd/SZ prepared through a 'one-pot' sol–gel route was investigated in relation to a dual-catalyst aftertreatment system where an NO/HC/CO oxidation catalyst (Co/ZrO_2) and a NOx reduction catalyst (Pd/SZ) were utilized to achieve improved aftertreatment efficiency under lean conditions. The dual-catalyst system was capable of achieving N_2 yields in excess of 95% and was found to be very active for elimination of unburned hydrocarbons and CO. An inhibitory effect of water vapor was observed on NOx reduction and CH_4 combustion over Pd/SZ which was completely reversible upon removal of water vapor from the system. NO_2 reduction experiments in the presence of water vapor showed that while it has no effect on NO_2 adsorption and conversion under reaction conditions, water vapor altered the product distribution in favor of NO, which is a product of partial reduction of NO_2. Temperature-programmed desorption studies showed significant inhibition of NO and CH_4 adsorption by H_2O on Pd/SZ while NO_2 was able to compete more effectively with water vapor. Results suggested that the competition between H_2O and NO, suppressing reduction of NO by blocking the sites for NO adsorption/conversion resulted in increased NO yields and decreased N_2 yields during SCR of NO_2. Incorporation of the NO oxidation catalyst component was observed to offset the effect of water vapor by oxidizing NO, and thus replenishing partially reduced NO_2. Time-on-stream studies showed that the dual-catalyst system was capable of retaining NOx reduction activity over a period of 40 h. Studies on the hydrothermal stability of sulfate species showed that sulfate species were hydrated upon water adsorption on the surface however, complete recovery of these species was observed upon dehydration of the surface. It was shown that decreased NOx reduction activity in the presence of water vapor resulted from competition between CH_4–NO and H_2O under reaction conditions rather than leaching of the sulfate species.

Acknowledgements

Financial support provided by Department of Energy is gratefully acknowledged. The authors also acknowledge NSF support for acquisition of the XPS system under NSF-DMR grant #0114098.

References

[1] G.R. Gerber, M.A. Devine, Power 147 (2003) 24–29.
[2] R.M. Heck, Catal. Today 53 (1999) 519–523.
[3] R.M. Heck, R.J. Farrauto, Appl. Catal. A: Gen. 221 (2001) 443–457.
[4] M. Iwamoto, H. Hamada, Catal. Today 10 (1991) 57–71.
[5] M. Iwamoto, H. Yahiro, Catal. Today 22 (1994) 5–18.
[6] M.D. Amiridis, T. Zhang, R.J. Farrauto, Appl. Catal. B: Environ. 10 (1996) 203–227.
[7] Y. Nishizaka, M. Misono, Chem. Lett. 22 (1993) 1295–1298.
[8] Y. Nishizaka, M. Misono, Chem. Lett. 23 (1994) 2237–2240.
[9] A. Ali, W. Alvarez, C.J. Loughran, D.E. Resasco, Appl. Catal. B 14 (1997) 13–22.
[10] R. Burch, Catal. Today 35 (1997) 27–36.
[11] H. Ohtsuka, T. Tabata, Appl. Catal. B: Environ. 21 (1999) 133–139.
[12] Y.-H. Chin, A. Pisanu, L. Serventi, W. Alvarez, D.E. Resasco, Catal. Today 54 (1999) 419–429.
[13] C. Descorme, P. Gelin, C. Lecuyer, M. Primet, Appl. Catal. B: Environ. 13 (1997) 185–195.
[14] C. Descorme, P. Gelin, C. Lecuyer, M. Primet, J. Catal. 177 (1998) 352–362.
[15] J.A.Z. Pieterse, R.W. Brink, S. Booneveld, F.A. de Bruijn, Appl. Catal. B: Environ. 39 (2002) 167–179.
[16] J. Suzuki, S. Matsumoto, Top. Catal. 28 (2004) 171–176.
[17] J.A.Z. Pieterse, H. Top, F. Vollink, K. Hoving, R.W. Brink, Chem. Eng. J. 120 (2006) 17–23.
[18] H. Ohtsuka, T. Tabata, T. Hirano, Appl. Catal. B: Environ. 28 (2000) L73–L76.
[19] C.E. Quincoces, S. Guerrero, P. Araya, M.G. Gonzalez, Catal. Commun. 6 (2005) 75–80.
[20] F. Figueras, B. Coq, E. Ensuque, D. Tachon, G. Delahay, Catal. Today 42 (1998) 117–125.
[21] Y.-H. Chin, W. Alvarez, D.E. Resasco, Catal. Today 62 (2000) 159–165.
[22] W. Suprun, K. Schaedlich, H. Papp, Chem. Eng. Technol. 28 (2005) 199–203.
[23] H. Ohtsuka, T. Tabata, Appl. Catal. B: Environ. 29 (2001) 177–183.
[24] C.M. De Correa, F. Cordoba, C.F.L. Bustamante, Stud. Surf. Sci. Catal. 130B (2000) 1469–1474.
[25] B. Wen, J. Jia, S. Li, T. Liu, L.X. Chenc, W.M.H. Sachtler, Phys. Chem. Chem. Phys. 4 (2002) 1983–1988.
[26] F. Bustamante, F. Córdoba, M. Yates, C.M.D. Correa, Appl. Catal. A: Gen. 234 (2002) 127–136.
[27] A.P. Ferreira, S. Capela, P.D. Costa, C. Henriques, M.F. Ribeiro, F.R. Ribeiro, Catal. Today 119 (2007) 156–165.
[28] M. Ogura, Y. Sugiura, M. Hayashi, E. Kikuchi, Catal. Lett. 42 (1996) 185–189.
[29] L.F. Cordoba, W.M.H. Sachtler, C.M.D. Correaa, Appl. Catal. B: Environ. 56 (2005) 269–277.
[30] E.M. Holmgreen, M.M. Yung, U.S. Ozkan, Appl. Catal. B: Environ. 74 (2007) 73–82.
[31] U.S. Ozkan, E.M. Holmgreen, M.M. Yung, Multi-stage catalyst systems and uses thereof, US 20,070,110,651.
[32] J. Despres, M. Elsener, M. Koebel, O. Krocher, B. Schnyder, A. Wokaun, Appl. Catal. B 50 (2004) 73–82.
[33] M.M. Yung, E.M. Holmgreen, U.S. Ozkan, J. Catal. 247 (2007) 356–367.
[34] E.M. Holmgreen, M.M. Yung, U.S. Ozkan, Catal. Lett. 111 (2006) 19–26.

[35] E.M. Holmgreen, M.M. Yung, U.S. Ozkan, J. Mol. Catal. A: Chem. 270 (2007) 101–111.
[36] K. Arata, Adv. Catal. 37 (1990) 165–212.
[37] J.F. Moulder, W.F. Stickle, P.E. Sobol, K.D. Bomben, Handbook of X-ray Photoelectron Spectroscopy, Perkin Elmer Corporation, Eden Prairie, 1992.
[38] R. Marcus, U. Diebold, R.D. Gonzalez, Catal. Lett. 86 (2003) 151–156.
[39] S. Ardizzone, C.L. Bianchi, E. Grassi, Colloid Surf. A 135 (1998) 41–51.
[40] C.L. Bianchi, S. Ardizzone, G. Cappalletti, Surf. Interface Anal. 36 (2004) 745–748.
[41] M. Hino, M. Kurashige, H. Matsuhashi, K. Arata, Themochim. Acta 411 (2006) 35–41.
[42] T. Tabata, M. Kokitsu, H. Ohtsuka, O. Okada, L.M.F. Sabatino, G. Bellussi, Catal. Today 27 (1996) 91–98.
[43] B.J. Adelman, T. Beutel, G.D. Lei, W.M.H. Sachtler, J. Catal. 158 (1996) 327–335.
[44] M.M. Yung, E.M. Holmgreen, U.S. Ozkan, Catal. Lett. 118 (2007) 180–186.
[45] M.M. Yung, Z. Zhao, M.P. Woods, U.S. Ozkan, J. Mol. Catal. A: Chem. 279 (2008) 1–9.
[46] C.F. Cullis, T.G. Nevell, D.L. Trimm, J. Chem. Soc. Farad. Trans. 1 (68) (1972) 1406–1412.
[47] R. Burch, D.J. Crittle, M.J. Hayes, Catal. Today 47 (1999) 229–234.
[48] F.H. Ribeiro, M. Chow, R.A. DallaBetta, J. Catal. 146 (1994) 537–544.
[49] F. Babou, G. Coudurier, J.C. Vedrine, J. Catal. 152 (1995) 341–349.
[50] C. Morterra, G. Cerrato, F. Pinna, M. Signoretto, J. Phys. Chem. 98 (1994) 12373–12381.
[51] C. Morterra, G. Cerrato, F. Pinna, M. Signoretto, G. Strukul, J. Catal. 149 (1994) 181–188.
[52] B. Li, R.D. Gonzalez, Catal. Today 46 (1998) 55–67.
[53] D. Ciuparu, M.R. Lyubovsky, E. Altman, L.D. Pfefferle, A. Datye, Catal. Rev. 44 (2002) 539–649.
[54] P. Forzatti, G. Groppi, Catal. Today 54 (1999) 165–180.
[55] P. Gelin, M. Primet, Appl. Catal. B: Environ. 39 (2002) 1–37.
[56] Y. Li, P.J. Battavio, J.N. Armor, J. Catal. 142 (1993) 561–571.